Int. J. Electrochem. Sci., 9 **(2014)** 3928 - 3950

International Journal of
ELECTROCHEMICAL
SCIENCE
www.electrochemsci.org

Electrochemical and Quantum Chemical Studies on Synthesized Phenylazopyrimidone Dyes as Corrosion Inhibitors for Mild Steel in a 15% HCl Solution

Mahendra Yadav[1,*], *Sushil Kumar*[1], *Indra Bahadur*[2], *Deresh Ramjugernath*[2,*]

[1]Department of Applied Chemistry, Indian School of Mines, Dhanbad, 826004, India
[2]Thermodynamics Research Unit, School of Engineering, University of KwaZulu-Natal, Howard College Campus, King George V Avenue, Durban, 4041, South Africa
[*]E-mail: yadav_drmahendra@yahoo.co.in, ramjuger@ukzn.ac.za

Received: 20 January 2014 / *Accepted:* 31 March 2014 / *Published:* 14 April 2014

The inhibition performance of synthesized phenylazopyrimidone dyes, namely, 3-(p-nitrophenylazo)-4-amino-1H- benzo[4,5]imidazo[1,2-a]pyrimidin-2-one (NABIP) and 3-(p-methoxyphenylazo)-4-amino-1H- benzo[4,5]imidazo[1,2-a]pyrimidin-2-one (MABIP) were investigated as corrosion inhibitors for mild steel in a 15% HCl solution using potentiodynamic polarization and electrochemical impedance spectroscopy (EIS) measurements. The inhibition efficiency of both inhibitors increased with an increase in the concentration of inhibitor. The inhibitors NABIP and MABIP at a concentration of 200 ppm at 303 K show corrosion inhibition efficiencies of 93.1 and 97.9%, respectively. Polarization studies showed that both inhibitors studied were of a mixed type in nature. The adsorption of inhibitors on the mild steel surface obeys the Langmuir adsorption isotherm. Scanning electron microscopy (SEM), energy dispersive spectroscopy (EDS), and atomic force microscopy (AFM) were performed for the surface study of the uninhibited and inhibited mild steel samples. Density functional theory (DFT) was employed for theoretical calculations.

Keywords: Mild steel; Corrosion inhibitor; EIS; Polarization; AFM; Acid inhibition; Density functional theory

1. INTRODUCTION

Mild steel, widely used in industrial applications, is highly susceptible to corrosion, especially in an acidic environment [1, 2]. With regard to acidic media, the use of hydrochloric acid solutions in acid pickling, industrial cleaning, acid descaling, and acidization of oil wells is more economical, efficient and trouble-free, compared to other mineral acids [3, 4]. Because of the strong corrosivity of acid solutions, inhibitors are commonly used to reduce the corrosive attack on metal surfaces. In recent

years, there has been a considerable amount of effort devoted to finding efficient corrosion inhibitors. It is well known that heterocyclic compounds, containing electronegative functional groups, π-electrons and heteroatoms like sulfur, nitrogen and oxygen as well as aromatic rings in their structures, often show good corrosion inhibitive performance in an acid environment [5–8]. The inhibiting action of these compounds is due to the adsorption of these compounds onto the metal/solution interface. The adsorption process depends upon the nature and surface charge of the metal, the type of aggressive media, the structure of the inhibitor and the nature of its interaction with the metal surface [12].

Azo compounds are the most widely used class of dyes due to their versatile application in various fields, such as the dyeing of textiles and fibers, colouring of different materials, and high-technology areas, such as electro-optical devices and ink-jet printers. A survey of literature reveals that organic dyes are quite effective in retarding the corrosion of mild steel and aluminum in acidic or basic environments [13-22].

As a continuation of our research on developing corrosion inhibitors [8-11] with high effectiveness and efficiency, the present paper explores a systematic study to ascertain the inhibitive action of synthesized phenylazopyrimidone dyes, namely, 3-(p-nitrophenylazo)-4-amino-1H-benzo[4,5]imidazo[1,2-a]pyrimidin-2-one (NABIP) and 3-(p-methoxyphenylazo)-4-amino-1H-benzo[4,5]imidazo[1,2-a]pyrimidin-2-one (MABIP) on corrosion of mild steel in a 15% HCl solution using potentiodynamic polarization, AC impedance and quantum chemical calculations.

2. EXPERIMENTAL PROCEDURES

2.1. Synthesis of inhibitors

Phenylazopyrimidone dyes, namely, 3-(p-Nitrophenylazo)-4-amino-1H-benzo[4,5]imidazo[1,2-a]pyrimidin-2-one (NABIP) and 3-(p-Methoxyphenylazo)-4-amino-1H-benzo[4,5]imidazo[1,2-a]pyrimidin-2-one (MABIP) were synthesized in our laboratory as per the reported procedure [23] as given in Scheme 1.

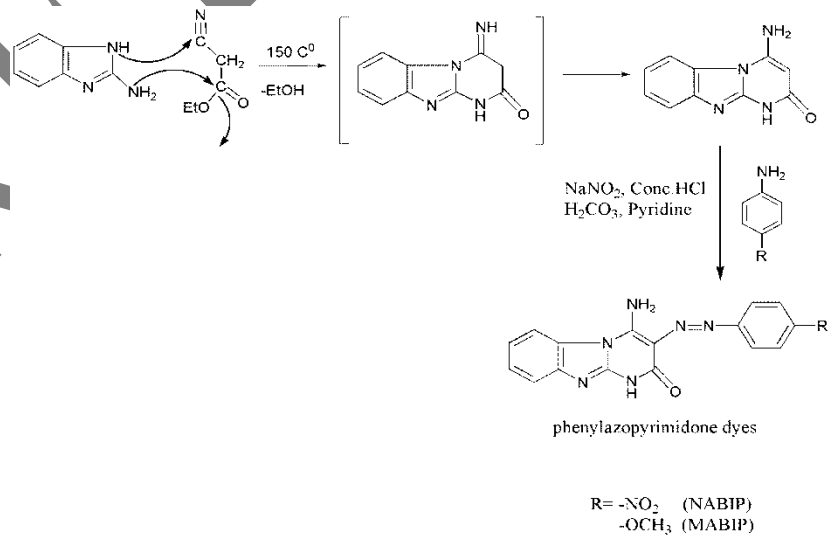

Scheme 1. Synthetic route for inhibitors, NABIP and MABIP.

The compound 4-amino-1H- benzo[4,5]imidazo[1,2-a]pyrimidin-2-one was synthesized by heating 2-aminobenzimidazole (1 g, 7.5 mmol) with ethyl cyanoacetate (5.10 g, 45 mmol) at 423 K with continuous stirring for 2 h in a round bottom flask. The compound obtained, 4-amino-1H-benzo[4,5]imidazo[1,2-a]pyrimidin-2-one, was cooled to 278 K in pyridine (10 mL) in a round bottom flask and added to a solution of carbocyclic diazonium chloride which was prepared from substituted aniline (1.5 mmol), sodium nitrite (1.5 mmol) and concentrated HCl (4 mL) in water, to obtain NABIP and MABIP. The purity of the synthesized inhibitors was confirmed by thin-layer chromatography (TLC). The structures of the synthesized inhibitors are shown in Figure 1.

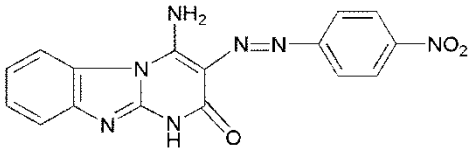

3-(p-Nitrophenylazo)-4-amino-1H-benzo[4,5]imidazo[1,2-a]pyrimidin-2-one (NABIP)

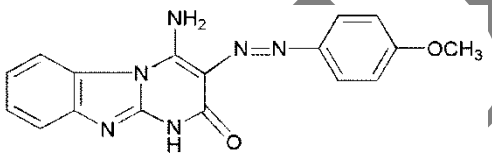

3-(p-Methoxyphenylazo)-4-amino-1H-benzo[4,5]imidazo[1,2-a]pyrimidin-2-one (MABIP)

Figure 1. Structure of inhibitors, NABIP and MABIP.

The structures of the synthesized dyes were confirmed by using the physico-chemical and spectroscopic data as given in Table 1.

Table 1. Physico – chemical and spectroscopic data of synthesized compounds.

Inhibitor	3-(p-Nitrophenylazo)-4-amino-1H-benzo[4,5]imidazo[1,2-a]pyrimidin-2-one (NABIP)	3-(p-Methoxyphenylazo)-4-amino-1H-benzo[4,5]imidazo[1,2-a]pyrimidin-2-one (MABIP)
Structure	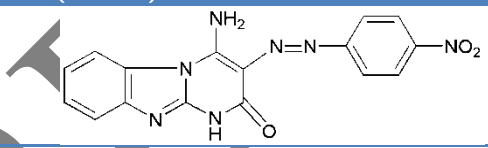	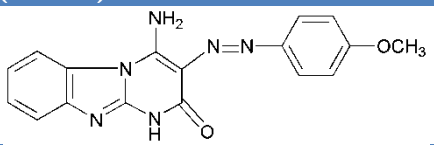
Analytical data	Color: brown crystal; Yield: 0.45 g, 86%; mp. dec. 315-320 °C; IR (KBr, cm^{-1}): *v* 3425, 3380(NH_2), 3130 (NH), 3080 (Aromatic-H), 1680 (C=O); ^{1}H NMR (DMSO-d_6): δ 10.72 (b, toutomeric NH_2), 9.85 (1H, b, NH), 9.15 (b, taotomeric NH), 8.55 (2H, m), 8.30 (2H, m) 8.25 (1H, m), 7.35 (1H, m), 7.45 (1H, m), 7.15 (1H, m).	Color: greenish yellow crystals; Yield: 0.40 g, 80%; mp. 293-295 °C; IR (KBr, cm^{-1}): *v* 3430, 3380 (NH_2), 3140 (NH), 3075 (Aromatic-H), 2870 (Aliphatic-H), 1680 (C=O), 1120 (C-O); ^{1}H NMR (DMSO-d_6): δ9.80 (b,tautomeric NH_2), 9.95 (1H, b, NH), 9.50 (b, tautomeric NH), 8.15 (1H,m), 7.25 (1H, m), 7.30 (1H, m) 6.45 (2H, m), 3.60 (3H, s).

2.2. Mild steel sample

Corrosion studies were performed on mild steel samples having composition (wt. %): C, 0.12; Mn, 0.11; Cu, 0.01; Si, 0.02; Sn, 0.01; P, 0.02; Ni, 0.02 and the balance Fe. For electrochemical measurements mild steel coupons having dimensions 1.0 cm × 1.0 cm × 0.1 cm were mechanically cut

and abraded with different grade emery papers (120, 220, 400, 600, 800, 1500 and 2000 grade). The coupons had an exposed area of 1 cm^2 (rest covered with araldite resin) with a 3 cm long stem. Prior to experiments, specimens were washed with distilled water, degreased in acetone, dried and stored in a vacuum desiccator.

2.3. Test solution

Analytical reagent (AR) grade HCl was diluted with triply distilled water to obtain a 15% HCl solution. The concentration of inhibitors employed was varied from 25 to 200 ppm (mg L^{-1}), and the volume of electrolyte used was 250 ml.

2.4. Methods

2.4.1. Electrochemical polarization method

Electrochemical polarization measurements were carried out in a conventional three-electrode cell consisting of a mild steel working electrode, a platinum counter electrode and a saturated calomel electrode (SCE) as a reference electrode, using a CH electrochemical workstation (Model No: CHI 760D, manufactured by CH Instruments, Austin, USA) at different temperatures. Mild steel samples were exposed (1cm^2) to various concentrations (25-200 ppm) of different inhibitors in a 15% HCl solution at different temperatures (303-333 K). After establishment of the open circuit potential, potentiodynamic polarization curves were obtained at a scan rate of 1.0 mVs^{-1} in the potential range from -700 to -300 mV vs SCE with respect to the open circuit potential. Corrosion current density (i_{corr}) was obtained by the Tafel extrapolation method. The percentage inhibition efficiency (η %) and surface coverage (θ) was calculated using the equations given below:

$$\eta(\%) = \frac{i^0_{corr} - i_{corr}}{i^0_{corr}} \times 100 \quad (1)$$

$$\theta = 1 - \frac{i_{corr}}{i^0_{corr}} \quad (2)$$

where i^0_{corr} and i_{corr} are the values of the corrosion current density in the absence and presence of inhibitors, respectively.

2.4.2. Electrochemical impedance spectroscopy method

Electrochemical impedance spectroscopy measurements were carried out using the same electrochemical cell and electrochemical workstation as mentioned for polarization measurements, in the frequency range from 100 kHz to 10 mHz using an amplitude of 10 mV peak to peak AC signal at the open-circuit potential. The impedance data were obtained by using Nyquist and Bode plots. The

inhibition efficiency (η %) was calculated from charge transfer resistance values obtained from impedance measurements using the following relation

$$\eta(\%) = \frac{R_{ct\,(inh)} - R_{ct}}{R_{ct\,(inh)}} \times 100 \qquad (3)$$

where $R_{ct(inh)}$ and R_{ct} are the charge transfer resistances in the presence and absence of inhibitor respectively. The value of the double layer capacitance (C_{dl}) was calculated from charge transfer resistance and CPE parameters (Y_0 and n) using the expression [24]

$$C_{dl} = (Y_0 R_{ct}^{1-n})^{1/n} \qquad (4)$$

where Y_0 is the CPE constant and n is the CPE exponent . The value of n represents the deviation from the ideal behavior and it lies between 0 and 1.

2.4.3. Scanning electron microscopic and energy dispersive spectroscopy analysis

Mild steel samples of size 1.0 cm × 1.0 cm × 0.1 cm were abraded with a series of emery paper (grade 320-500-800-1200) and then washed with distilled water and acetone. After immersion in a 15% HCl solution in the absence and presence of an optimum concentration (200 ppm) of inhibitors (NABIP, MABIP) at 303 K for 6 h, the sample was washed with distilled water, dried with a cold air blaster, and then EDS and SEM images were recorded using a Traktor TN-2000 energy dispersive spectrometer and JEOL JSM – 6380 LA analytical scanning electron microscope in the vacuum mode with the instrument operated at 10 kV.

2.4.4. Atomic Force Microscopy

The surface morphology of the uninhibited and inhibited mild steel samples was investigated by atomic force microscopy (AFM). For AFM analysis the mild steel samples of size 1 cm × 1 cm × 0.1 cm were immersed in the test solution in the absence and presence of an optimum concentration (200 ppm) of the inhibitors for 6 h at 303 K. After 6 h immersion, the samples were taken out from the solution, washed with distilled water, dried, and used for AFM. The AFM studies were carried out using a Nanosurf Easyscan2 Instrument, Model: NT-MDT, Russia; Solver Pro-47.

2.4.5. Quantum chemical study

Complete geometrical optimizations of the investigated molecules were performed using density functional theory (DFT) with the Beck's three parameter exchange functional along with the Lee–Yang–Parr nonlocal correlation functional (B3LYP), with the 6-31G (d, p) basis set implemented in the Gaussian 03 program package [25, 26]. Theoretical parameters such as the energies of the

highest occupied and lowest unoccupied molecular orbital (E_{HOMO} and E_{LUMO}), energy gap (ΔE), absolute electronegativity (χ), dipole moment (μ), global hardness (γ) and softness (σ), and fraction of electrons transferred (ΔN) were calculated.

3. RESULTS AND DISCUSSION

3.1. Electrochemical Studies

3.1.1. Polarization studies

The potentiodynamic polarization curves for the mild steel in a 15% HCl solution at 303 K, in the absence and presence of different concentrations of NABIP and MABIP, are shown in Figure 2 (a, b).

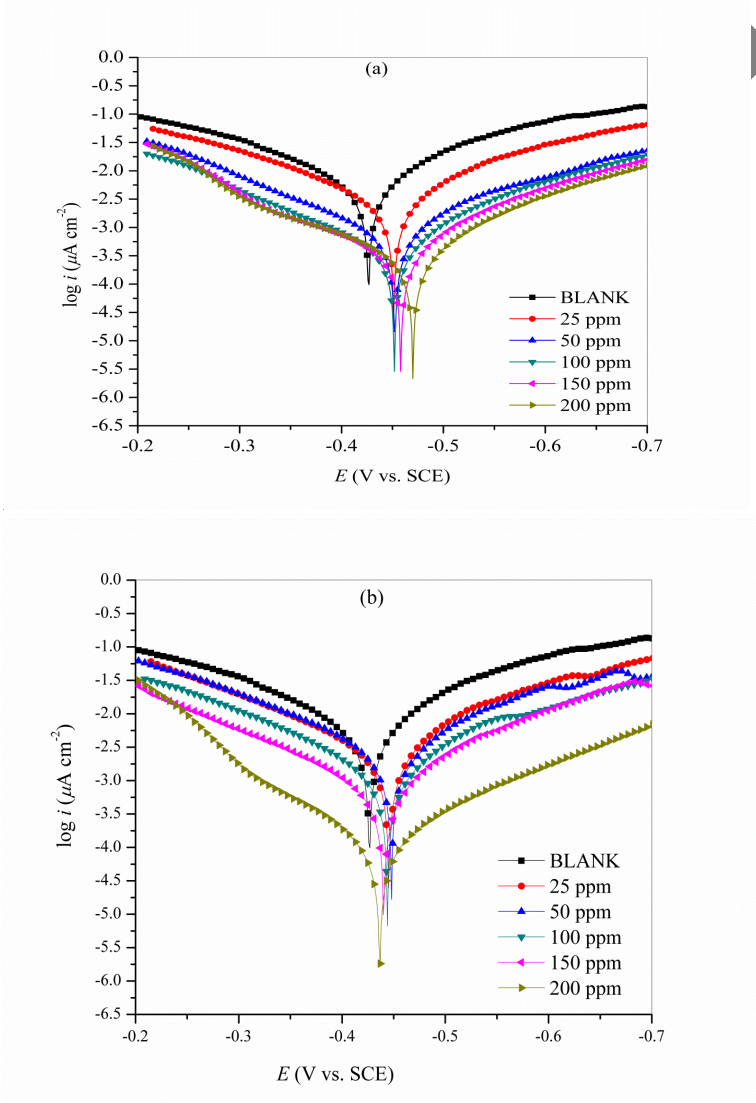

Figure 2. Potentiodynamic polarization curves for mild steel in a 15% HCl solution in the presence and absence of inhibitor at 303K (a) NABIP (b) MABIP.

It is apparent from Figure 2 (a, b) that the nature of the polarization curves remain almost the same in the absence and presence of inhibitors, but the anodic and cathodic curves are shifted toward a lower current density in the presence of inhibitors, indicating that the addition of inhibitor reduces the mild steel anodic dissolution and also retards the hydrogen ions reduction, and this inhibition effect is enhanced with an increase in the inhibitor's (NABIP and MABIP) concentration, which may be due to the adsorption of inhibitor on the electrode surface [27,28]. The corrosion current densities were calculated by extrapolation of linear sections of the anodic and cathodic curves to the corrosion potential. The corrosion parameters such as corrosion potential (E_{corr}), anodic Tafel slope (β_a), cathodic Tafel slope (β_c), corrosion current density (i_{corr}), and percentage inhibition efficiency (η %) obtained from these curves are given in Table 2.

Table 2. Corrosion parameters for mild steel in a 15% HCl solution in the absence and presence of different concentrations of inhibitors obtained from electrochemical measurements at 303 K.

Inhibitor	Conc. (ppm)	$-E_{corr}$ (mV/SCE)	i_{corr} (μA cm^{-2})	β_a (mV dec^{-1})	β_c (mV dec^{-1})	θ	η(%)
Blank	0	416	6733	332	338	-	-
NABIP	25	438	3341	328	328	0.50	50.4
	50	495	2185	348	319	0.67	67.5
	100	498	1409	443	334	0.79	79.1
	150	437	1021	334	362	0.84	84.8
	200	449	466	380	294	0.93	93.1
MABIP	25	425	3178	349	375	0.52	52.8
	50	440	1588	358	351	0.76	76.4
	100	432	1232	325	341	0.81	81.7
	150	429	927	337	324	0.86	86.2
	200	433	140	283	312	0.97	97.9

The results reveal that increasing the concentration of both inhibitors results in a decrease in the corrosion current densities and an increase in the inhibition efficiency (η %), suggesting the adsorption of inhibitor molecules at the surface of mild steel to form protective film, resulting in retardation of metal dissolution [29]. The anodic Tafel slope (β_a) and the cathodic Tafel slope (β_c) of NABIP and MABIP changed with inhibitor concentration, indicating that these inhibitors control both anodic as well as cathodic reactions and act as mixed inhibitors. The presence of inhibitor causes a minor change in E_{corr} values with respect to the E_{corr} value in the absence of inhibitor. This implies that the inhibitor acts as a mixed type inhibitor, affecting both anodic and cathodic reactions [30]. If the displacement in E_{corr} is more than ±85 mV vs SCE relating to corrosion potential of the blank, the inhibitor acts as a pure cathodic or anodic type [31]. If the change in E_{corr} is less than 85 mV vs SCE, the corrosion inhibitor acts as a mixed type. The maximum displacement in E_{corr} in our study was found to be 71 mV

indicating that NABIP and MABIP act as mixed type inhibitors. The minor shift in E_{corr} toward a negative potential for both the inhibitors indicates that these inhibitors act as mixed inhibitors with more tendency toward a cathodic nature.

Corrosion inhibition studies were also carried out at different temperatures ranging from 303 K to 333 K. Corrosion parameters namely, surface coverage (θ) and inhibition efficiency (η %) of mild steel in a 15% HCl solution in the absence and presence of an optimum concentration (200 ppm) of inhibitors at different temperatures (303 K- 333K), obtained from polarization measurements are shown in Table 3.

Table 3. Corrosion parameters of mild steel in a 15% HCl solution in the absence and presence of optimum concentration (200 ppm) of inhibitors at different temperature, obtained from electrochemical measurements.

Inhibitor	Temp (K)	$-E_{corr}$ (mV/SCE)	i_{corr} (μA cm^{-2})	β_a (mVdec^{-1})	β_c (mV dec^{-1})	θ	η(%)
Blank	303	416	6733	332	338	-	-
	313	419	11720	382	453	-	-
	323	426	31550	459	437	-	-
	333	464	34870	450	460	-	-
NABIP	303	449	466	380	294	0.92	93.1
	313	428	2552	386	371	0.78	78.2
	323	429	9420	435	422	0.70	70.1
	333	525	16680	408	391	0.52	52.2
MABIP	303	433	140	283	312	0.97	97.9
	313	616	1681	437	338	0.85	85.7
	323	452	7225	482	388	0.77	77.1
	333	514	15975	532	366	0.54	54.2

It is clear from the Table 3 that the corrosion rate increases with an increase in temperature in the presence and absence of the inhibitors. The inhibition efficiency decreases with an increasing temperature from 303 to 333 K, indicating that at higher temperatures dissolution of mild steel predominates on inhibitor adsorption [32]. Such type of behavior can also be described on the basis that the increase in temperature leads to a shift of the equilibrium constant towards desorption of the inhibitor molecules at the surface of mild steel [33].

3.1.2. EIS studies

The Nyquist plots for mild steel obtained at the interface in a 15% HCl solution with and without the different concentrations of NABIP and MABIP at 303 K are shown in Figure 3 (a, b).

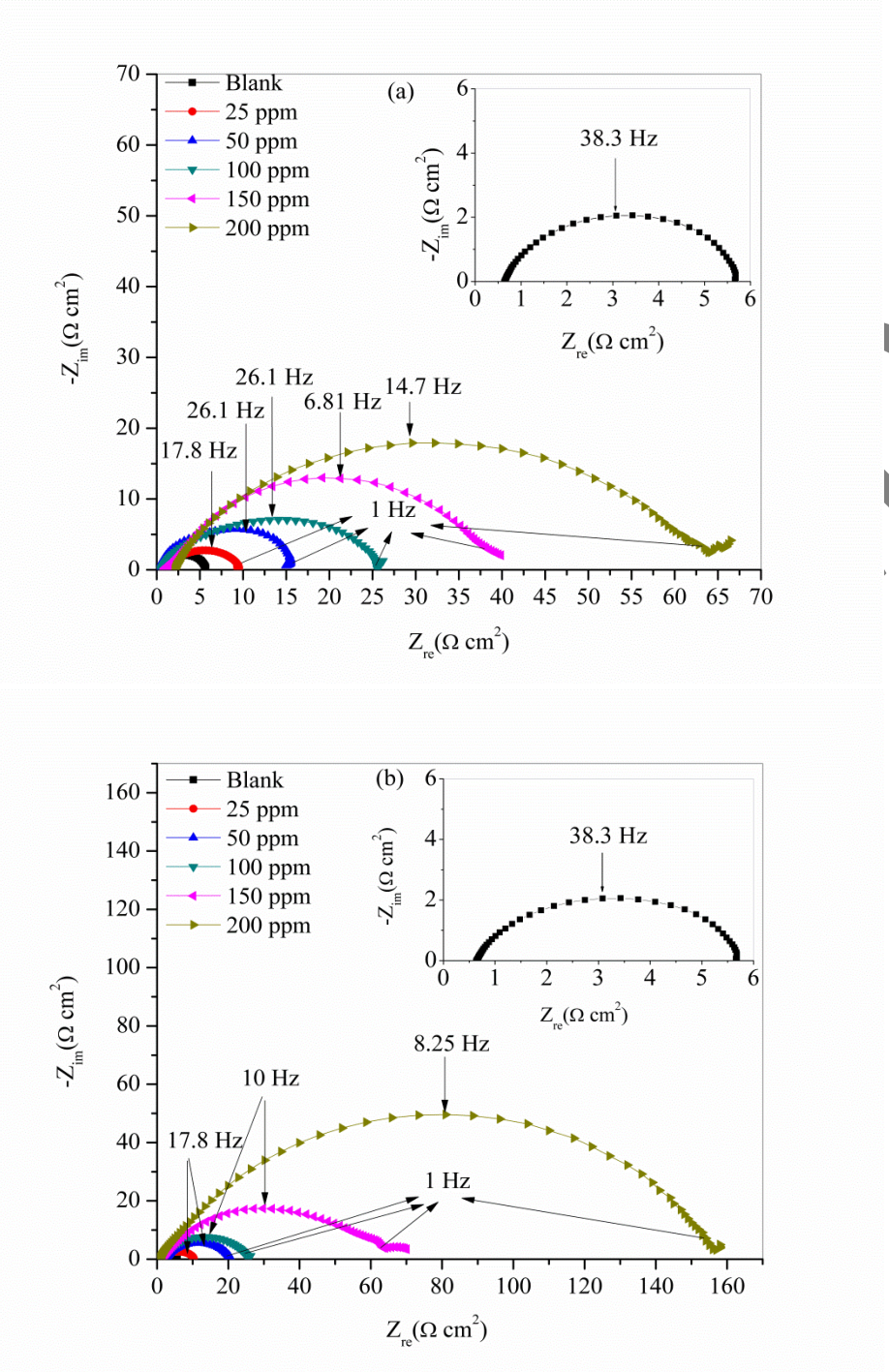

Figure 3. Nyquist plot for mild steel in a 15% HCl solution containing various concentrations of (a) NABIP (b) MABIP at 303 K.

The best fitting of experimental data is represented by Randles equivalent circuit (Fig. 4), which is a parallel combination of the charge-transfer resistance (R_{ct}) and the constant phase element (CPE), both in series with the solution resistance (R_s). This type of electrochemical equivalent circuit was reported previously to model the iron/acid interface [34].

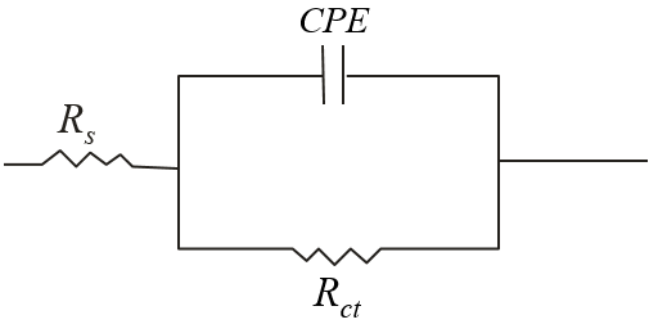

Figure 4. Equivalent circuit applied for fitting of the impedance spectra.

Table 4. Fitting results of EIS data for mild steel in a 15% HCl solution in the absence and presence of NABIP and MABIP at 303 K.

Inhibitors	Conc.(ppm)	R_s (Ω cm^2)	R_{ct} (Ω cm^2)	Y_o(μF cm^{-2})	N	C_{dl} (μF cm^{-2})	η%
Blank	-	0.65	5.1	254	0.81	53.3	-
NABIP	25	0.94	9.9	140	0.81	29.9	48.5
	50	0.31	16.2	73	0.83	18.4	68.5
	100	0.47	25.6	61	0.84	17.8	80.1
	150	1.92	36.2	24	0.87	8.4	85.9
	200	1.96	57.8	12	0.91	5.8	91.2
MABIP	25	0.83	11.2	113	0.82	26.1	54.5
	50	2.09	21.2	63	0.84	17.8	75.9
	100	0.86	27.4	52	0.85	16.3	81.4
	150	1.14	62.3	17	0.87	6.1	91.8
	200	0.66	155.1	8	0.93	4.8	96.7

As it can be seen from Figure 3 (a, b), the Nyquist plots contain depressed semicircles with the centre under the real axis (Z_{re}). Such behavior is characteristic for solid electrodes and often referred to frequency dispersion, could be attributed to different physical phenomena such as roughness and inhomogeneities of the solid surfaces, impurities, grain boundaries and distribution of the surface active sites [35-37]. Therefore, a constant phase element (CPE) was introduced in the circuit instead of a pure double layer capacitor (C_{dl}) to provide a more accurate fit of the experimental data. The impedance function of a CPE is defined by the mathematical expression given below [38]

$$Z_{CPE} = [Y_0(j\omega)^n]^{-1} \qquad (5)$$

where Y_0 is the magnitude of the CPE, n the CPE exponent (phase shift), j is the imaginary number ($j^2 = -1$) and ω is the angular frequency ($\omega = 2\pi f_{max}$) for which the imaginary component of

impedance is maximum. When the value of n is 1, the CPE behaves like an ideal double-layer capacitance (C_{dl}).

The impedance data such as solution resistance (R_s), charge transfer resistance (R_{ct}), double layer capacitance (C_{dl}), CPE constants Y_0 and n obtained from fitted spectra are listed in Table 4.

The data shown in Table 4 reveals that the values of R_{ct} increase with addition of inhibitors as compared to the blank solution. The increase in values is attributed to the formation of an insulating protective film at the metal/solution interface [30]. The C_{dl} value decreases as we increase the concentration of both inhibitors. The decrease in C_{dl}, which is the result of a decrease in local dielectric constant and/or an increase in the thickness of the electrical double layer, suggests that the inhibitor molecules act by adsorption at the metal/solution interface [39]. The single peak obtained in the phase angle Bode plots (Fig.5 a, c) for both inhibitors indicates that the electrochemical impedance measurements fit well in a one-time constant equivalent model (Randle's cell model) with constant phase element (CPE). Figure 5 (b, d) shows that the impedance value in the presence of both inhibitors is larger than in the absence of inhibitors and the value of impedance increases with an increase in the concentration of both inhibitors studied. This means that the corrosion rate is reduced in the presence of the inhibitors and continues to decrease with an increase in the concentration of inhibitors. The electrochemical impedance results (η %) are in good agreement with the results (η %) obtained by potentiodynamic polarization experiments.

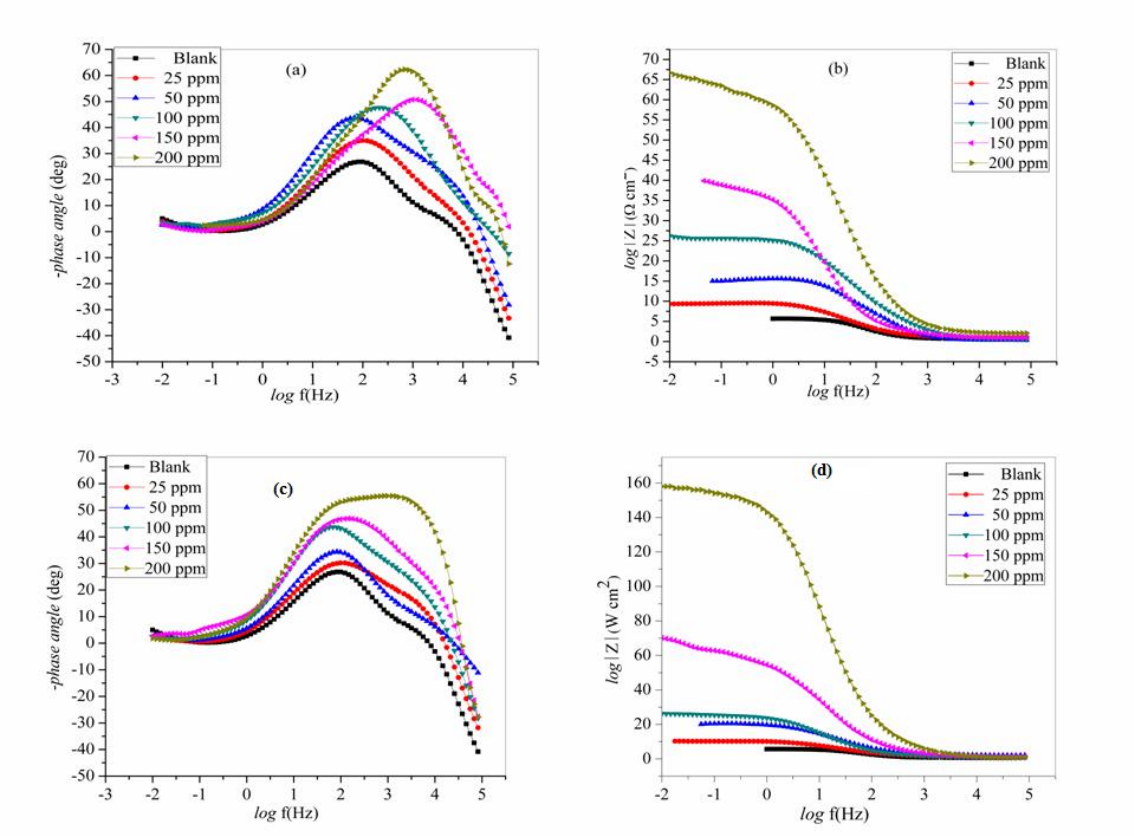

Figure 5. Bode plots for mild steel in a 15% HCl solution in the absence and presence of different concentrations of inhibitors (a, b) NABIP (c, d) MABIP.

3.2. Thermodynamic and activation parameters

The apparent activation energy (E_a) for dissolution of mild steel in a 15% HCl solution was calculated using the Arrhenius equation.

$$\log i_{corr} = \frac{-E_a}{2.303RT} + \log A \quad (6)$$

where, R is the molar gas constant (8.314 J $K^{-1}mol^{-1}$), T is the absolute temperature (K) and A is the Arrhenius pre-exponential factor. Figure 6 presents the Arrhenius plot of log i_{corr} against 1/T for the corrosion of mild steel in a 15% HCl solution in the absence and presence of an optimum concentration (200 ppm) of NABIP and MABIP inhibitors.

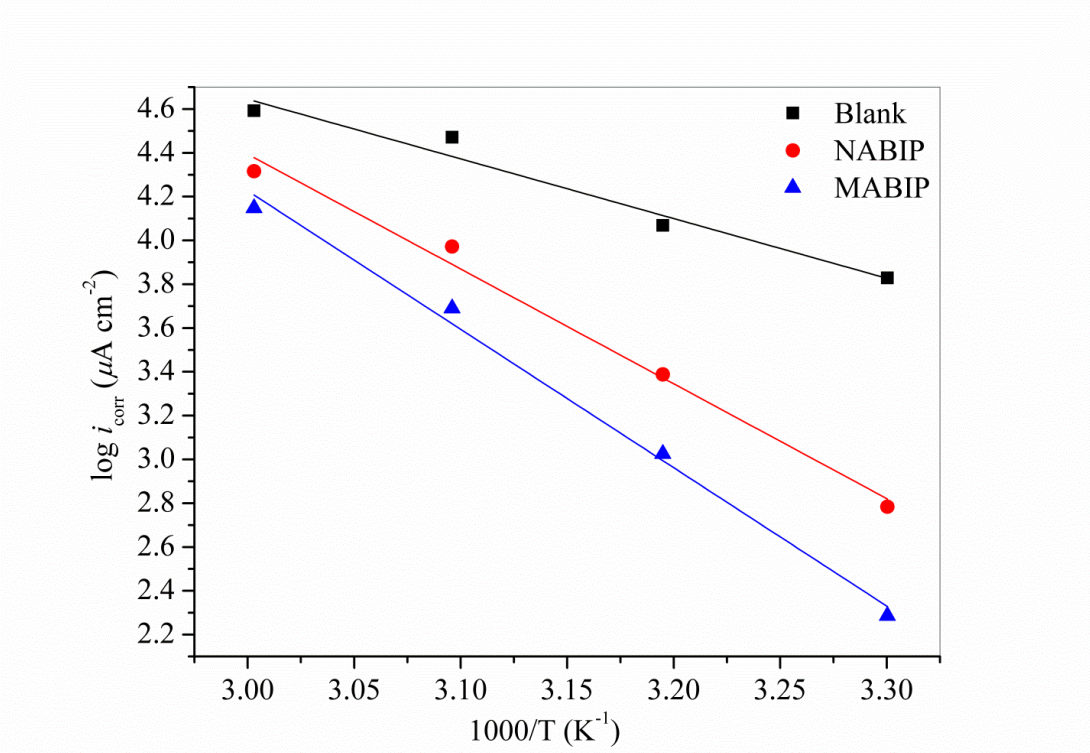

Figure 6. Arrhenius plots for mild steel corrosion in a 15% HCl solution for NABIP and MABIP.

From Figure 6, the slope of each individual line was determined, and the activation energy was calculated using the expression E_a = - (slope) × 2.303R. The calculated values of E_a are summarized in Table 5. It is evident from Table 5 that the values of the apparent activation energy for the inhibited solutions were higher than that for the uninhibited solution, indicating that the dissolution of mild steel was decreased due to the formation of a barrier by the adsorption of the inhibitors on mild steel surface [40, 41].

The values of standard enthalpy of activation (ΔH^*) and standard entropy of activation (ΔS^*) were calculated using the equation

$$i_{corr} = \frac{RT}{Nh}\exp\left(\frac{\Delta S^*}{R}\right)\exp\left(-\frac{\Delta H^*}{RT}\right) \quad (7)$$

where, h is Planck's constant and N is the Avogadro number, respectively.

A plot of log (i_{corr}/T) against $1/T$ (Fig. 7) in the presence of 200 ppm concentration of NABIP and MABIP gave straight lines with a slope of $-\Delta H^*/2.303R$ and an intercept of [$\log(R/Nh)$ + ($\Delta S^*/2.303R$)], from which the activation thermodynamic parameters (ΔH^* and ΔS^*) were calculated, as listed in Table 5.

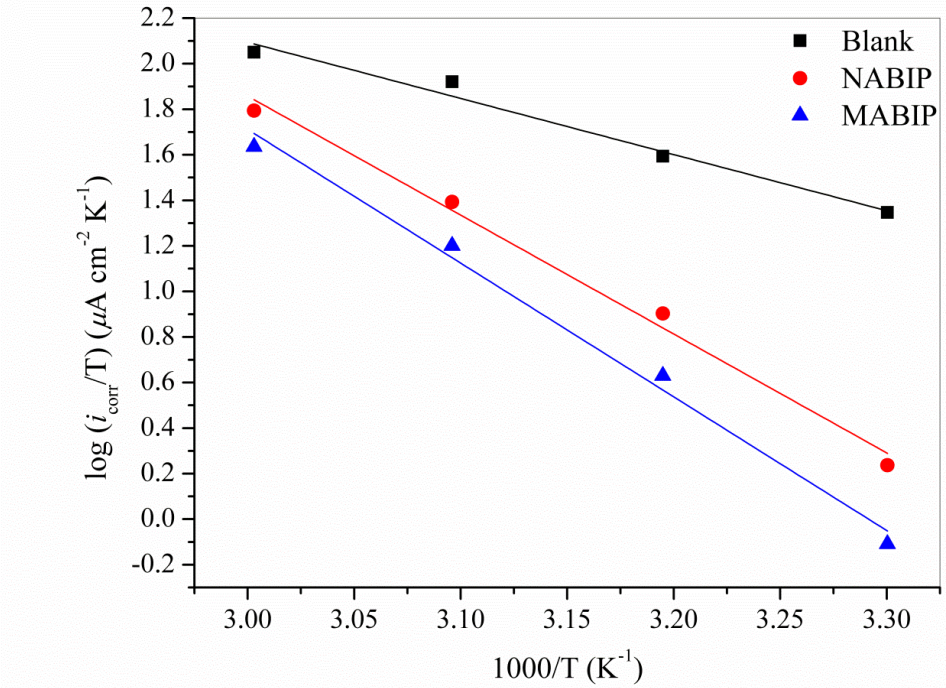

Figure 7. Transition state plot for mild steel in a 15% HCl solution at different concentration of NABIP and MABIP.

Table 5. Activation parameters for mild steel in a 15% HCl solution in the absence and presence of an optimum concentration (200 ppm) of inhibitors obtained from electrochemical measurements.

Inhibitor	E_a (kJ mol^{-1})	ΔH^* (kJ mol^{-1})	ΔS^* (J mol^{-1}K^{-1})
Blank	52	51	-15.9
NABIP	100	99	-137.4
MABIP	121	112	-172.4

The positive sign of the enthalpy reflects the endothermic nature of the mild steel dissolution process [42, 43]. The negative value of ΔS^* for both inhibitors indicates that the formation of the activated complex in the rate determining step represents an association rather than a dissociation step, meaning that a decrease in disorder takes place during the course of the transition from reactants to activated complex [44].

3.3. Adsorption isotherm

The most commonly used adsorption isotherms are Langmuir, Temkin, and Frumkin isotherms. The surface coverage (θ) for different concentrations of inhibitors in a 15% hydrochloric acid was tested graphically by fitting a suitable adsorption isotherm. Plotting C_{inh}/θ vs. C_{inh} for NABIP and MABIP yielded a straight line [Fig. 8] with correlation coefficient (R^2) values at 303 K given in Table 6.

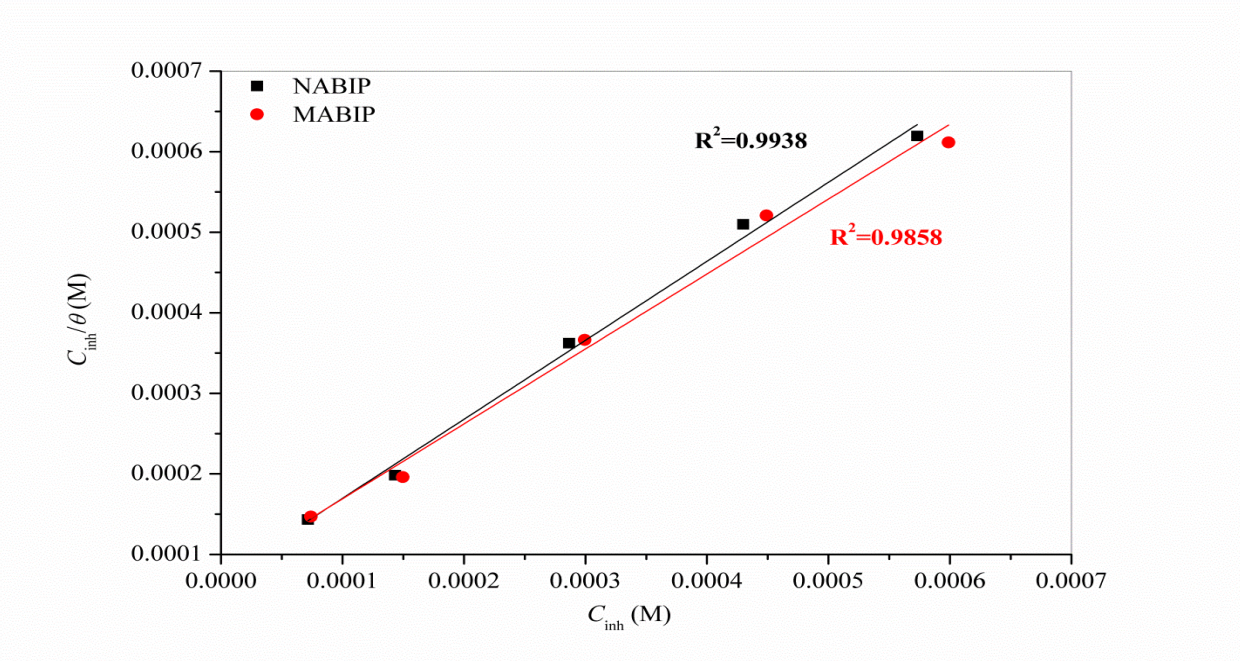

Figure 8. Langmuir plots for NABIP and MABIP.

The R^2 values in Table 6 are near unity indicating that the adsorption of both the inhibitors obey the Langmuir adsorption isotherm represented by the following equation.

$$\frac{C_{inh}}{\theta} = \frac{1}{K_{ads}} + C_{inh} \qquad (8)$$

where, C_{inh} is the inhibitor concentration, K_{ads} is the equilibrium constant for the adsorption-desorption process. The slope values for both inhibitors (Table 6) were found to be very close to unity, confirming the validity of Langmuir adsorption isotherms. From the intercept of Figure 8, the values of

K_{ads} were calculated and are listed in Table 6. Large values of K_{ads} obtained for both inhibitors studied imply more efficient adsorption and hence better corrosion inhibition efficiency. Using the values of K_{ads}, the values of ΔG°_{ads} were obtained using the following equation

$$\Delta G^{0}_{ads} = -RT \ln\left(55.5 K_{ads}\right) \quad (9)$$

The value of 55.5 is the concentration of water in solution in mol L^{-1}. Calculated values of K_{ads} and ΔG°_{ads} are listed in Table 6. In general, values of ΔG°_{ads} up to −20 $kJmol^{-1}$ are compatible with the electrostatic interaction between the charged inhibitor molecules and the charged metal surface (physisorption) and those which are more negative than −40 $kJmol^{-1}$ involve charge sharing or charge transfer from the inhibitor molecules to the metal surface (chemisorptions) [44]. The calculated ΔG°_{ads} values for NABIP and MABIP were -34.2 and -35.1 $kJmol^{-1}$, respectively, at 303 K, were between the threshold values for physical adsorption and chemical adsorption, indicating that the adsorption process of inhibitors on the mild steel surface involve both physical as well as chemical adsorption. Quraishi and Shukla [45] studied 4-substituted anilinomethylpropionate compounds as corrosion inhibitors for mild steel in a hydrochloric acid solution. The Gibbs free energy of adsorption for these molecules was reported to be approximately-38 $kJmol^{-1}$. They concluded that the adsorption mechanism for these molecules on steel involved two types of interactions, chemisorptions and physisorption. A similar conclusion was also reported by Ozcan [46] who studied the use of cystine as a corrosion inhibitor for mild steel in sulfuric acid. Thus, the calculated values of ΔG°_{ads} (Table 6) for both the inhibitors suggests that the adsorption of these inhibitors at the surface of mild steel is not pure physisorption or chemisorption, but it is combination of physisorption as well as chemisorptions.

The inhibition efficiency of NABIP and MABIP against the corrosion of mild steel in 15% HCl solution can be explained on the basis of the number of adsorption sites, their charge density, molecular size, mode of interaction with the metal surface and ability to form a metallic complex. Owing to the acidity of the medium, both the inhibitors either exist as a neutral species or in the protonated (cationic) form. In case of neutral species , the adsorption of the studied dyes on the metal surface is probably through the nitrogen atoms of the imidazole ring, pyrimidine ring, NH_2 group, N=N group and oxygen of pyrimidine ring, in addition to the delocalized π-electrons in the aromatic system. Moreover, these compounds may also adsorb through the electrostatic interactions between the protonated form (acid form) and the negatively charged metal surface.

The inhibitors NABIP and MABIP have nearly the same size and number of active centers, the difference is only that MABIP contains a $–OCH_3$ group and NABIP contains a $–NO_2$ group on the phenyl ring attached to the N=N group, however MABIP shows higher inhibition efficiency than NABIP due to higher delocalized π-electron density at the phenyl ring attached to the N=N group, which causes strong adsorption of MABIP at the surface of mild steel. The delocalized π-electron density at the phenyl ring attached to the N=N group in case of MABIP is more than in case of NABIP due to electron donating nature of the methoxy ($–OCH_3$) group and electron withdrawing nature of the nitro ($–NO_2$) group. Thus, inhibition efficiency of MABIP is higher due to the presence of methoxy

substituent having a +I effect and an inhibition efficiency of NABIP lower due to the presence of a nitro substituent with a –I effect.

Table 6. Adsorption parameters for NABIP and MABIP calculated from Langmuir adsorption isotherm for mild steel in a 15% HCl solution at 303 K.

Inhibitor	Temperature (K)	Slope	K_{ads} (M^{-1})	R^2	ΔG°_{ads} (kJ/mol)
NABIP	303	0.97	1.39×10^4	0.9938	-34.2
MABIP	303	0.98	1.96×10^4	0.9858	-35.1

3.4. Scanning electron microscopy

The surface morphology of the mild steel samples in a 15% HCl solution in the absence and presence of 200 ppm of NABIP and MABIP are shown in Figure 9 (a, b c, d).

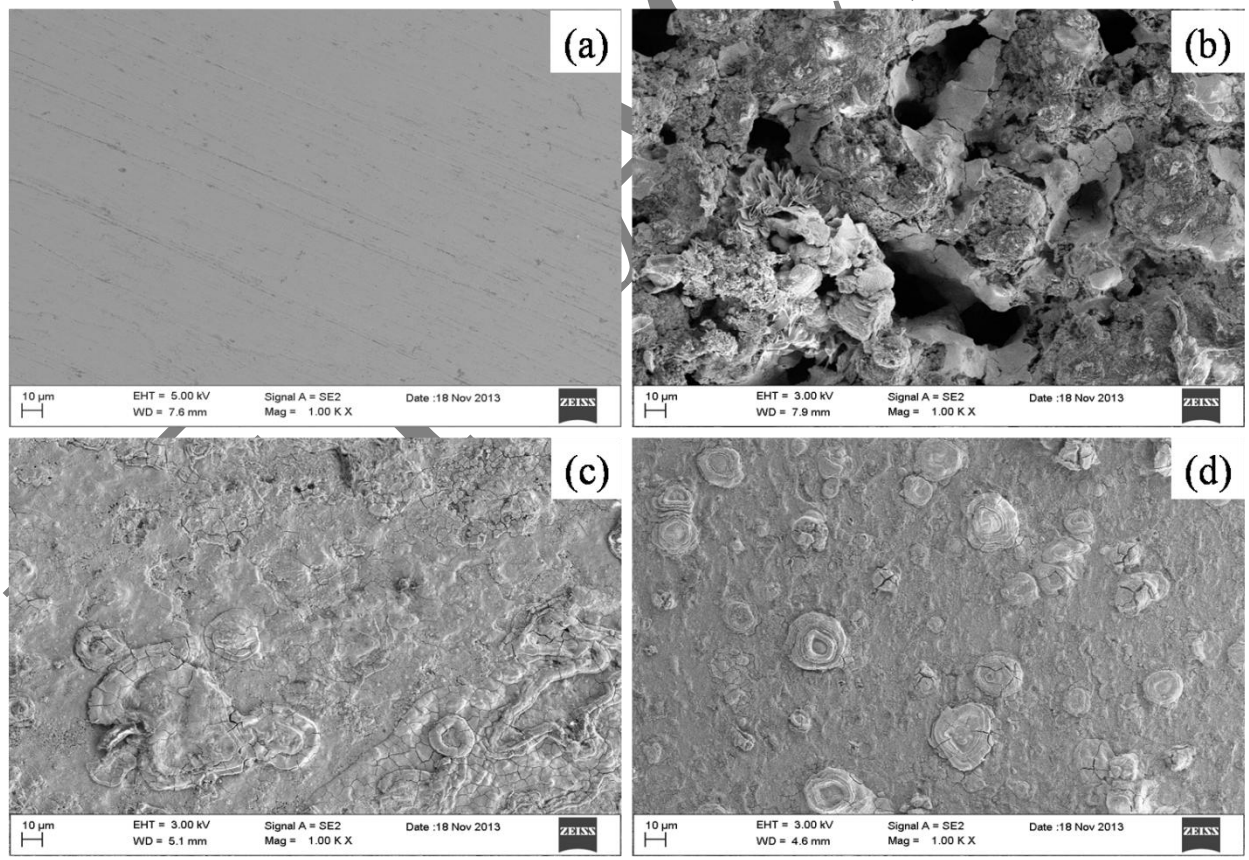

Figure 9. SEM images of mild steel in a 15% HCl solution after 6 h immersion at 303 K (a) before immersion (polished) (b) After immersion without inhibitor (c) in presence of inhibitor NABIP (d) in presence of inhibitor MABIP.

Figure 9 a, is SEM of a mild steel sample before immersion in a 15% HCl solution. The badly damaged surface (Fig. 9 b) obtained when the metal was kept immersed in a 15% HCl solution for 6 h without inhibitor indicates significant corrosion. However, in the presence of inhibitors (Fig. 9 c, d) the surface has remarkably improved with respect to its smoothness as compared to Fig. 9 b, indicating considerable reduction of the corrosion rate. This improvement in surface morphology is due to the formation of a protective film of inhibitor on the mild steel surface which is responsible for inhibition of corrosion.

3.5. Energy dispersive spectroscopy

The results of EDS spectra are shown in Figure 10 (a, b, c, d). Figures 10 (a) and (b) represent the EDS spectra of abraded and uninhibited mild steel specimens and Figures 10 (c) & (d) depicts inhibited mild steel specimens. The abraded mild steel specimen show characteristic peaks for elements (C, Mn, Cr, Si, Fe) constituting the mild steel sample. The EDS spectra of the uninhibited mild steel sample (Fig. 10 b) show a peak corresponding to Cl in addition to the abraded sample peaks.

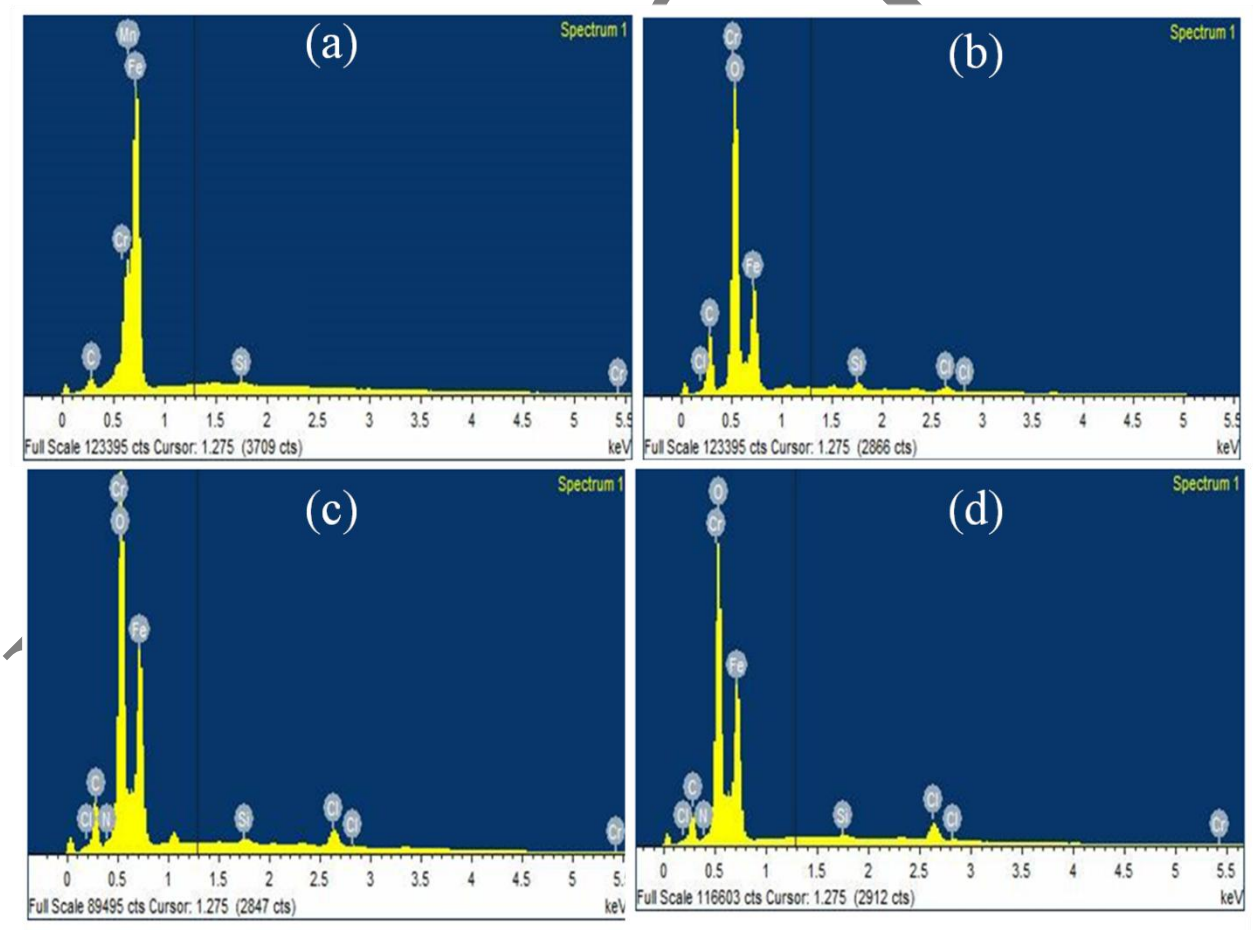

Figure 10. EDS spectra of mild steel specimens (a) polished (b) After immersion without inhibitor (c) with 200 ppm NABIP (d) with 200 ppm MABIP.

The EDS spectra of inhibited mild steel contains the peaks corresponding to all the elements present in the inhibitor molecules in addition to the uninhibited sample, indicating the adsorption of inhibitor molecules at the surface of mild steel. In addition to that, EDS of inhibited spectra shows that the Fe peaks are considerably suppressed as compared to the abraded and uninhibited mild steel sample. The suppression of the Fe lines might be due to an overlying inhibitor film. This indicates that the mild steel surface was covered with protective film of inhibitor molecules.

3.6. Atomic force microscopy

Surface morphology of the polished mild steel sample and mild steel sample in a 15% HCl solution in the absence and presence of inhibitors was investigated by atomic force microscopy (AFM). The results are shown in Figure 11 (a–d).

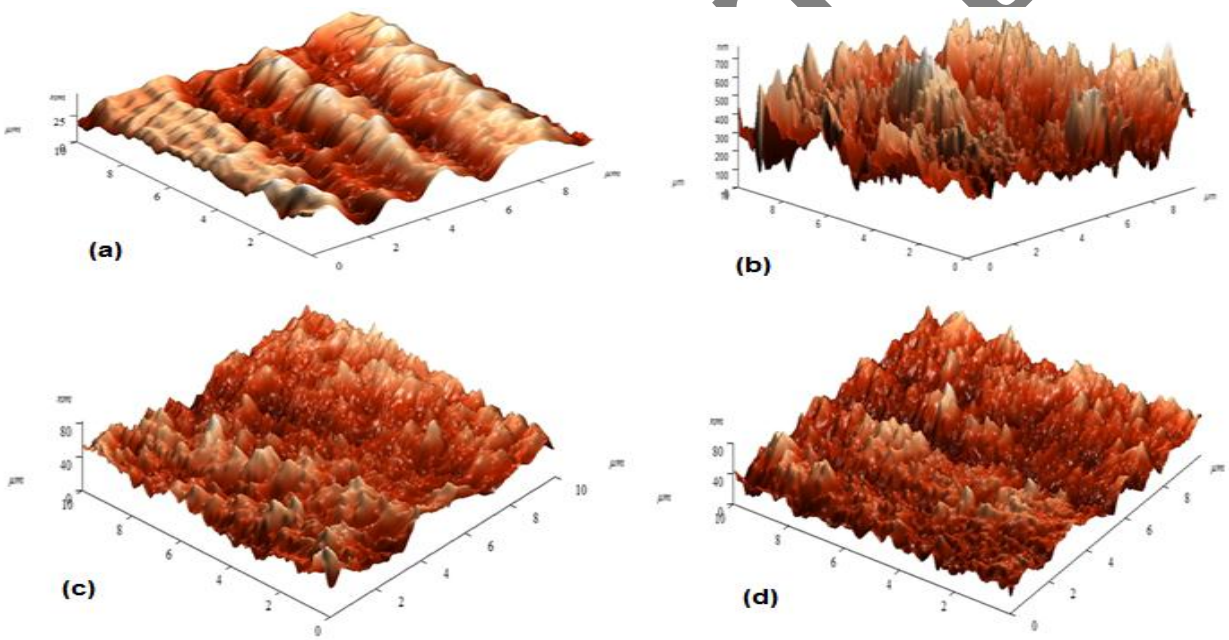

Figure 11. AFM micrograph of mild steel surface (a) polished mild steel (b) mild steel in a 15 % HCl solution (c) in presence of 200 ppm NABIP(d) in presence of 200 ppm MABIP.

The average roughness of the polished mild steel sample (Fig. 11a) and mild steel sample in a 15% HCl solution without inhibitor (Fig. 11 b) were found as 20 and 420 nm. It is clearly shown in Figure 11(b) that mild steel sample is badly damaged due to the acid attack on the surface. However, in the presence of an optimum concentration (200 ppm) of NABIP and MABIP as shown in Figure 11 (c, d), the average roughness was reduced to 50 and 40 nm, respectively. The lower value of roughness for MABIP compared to NABIP reveals that MABIP protects the mild steel surface more efficiently than NABIP in a 15% HCl solution.

3.7. Theoretical calculation

The optimized structure of NABIP and MABIP in its ground state is shown in Figure 12(a, b). The reactivity of a chemical species is well-defined in terms of frontier orbitals: the highest occupied molecular orbital (HOMO) and the lowest unoccupied molecular orbital (LUMO). According to the frontier molecular orbital (FMO) theory of chemical reactivity, the formation of a transition state is due to interaction between HOMO and LUMO of reacting species. The smaller the orbital energy gap (ΔE) between the participating HOMO and LUMO, the stronger will be the interactions between two reacting species [47].

It was reported previously by some researchers that smaller values of Δ*E* and higher values of dipole moment (μ) are responsible for higher inhibition efficiency [48]. According to HSAB theory, hard acids prefer to co-ordinate to hard bases and soft acid to soft bases.

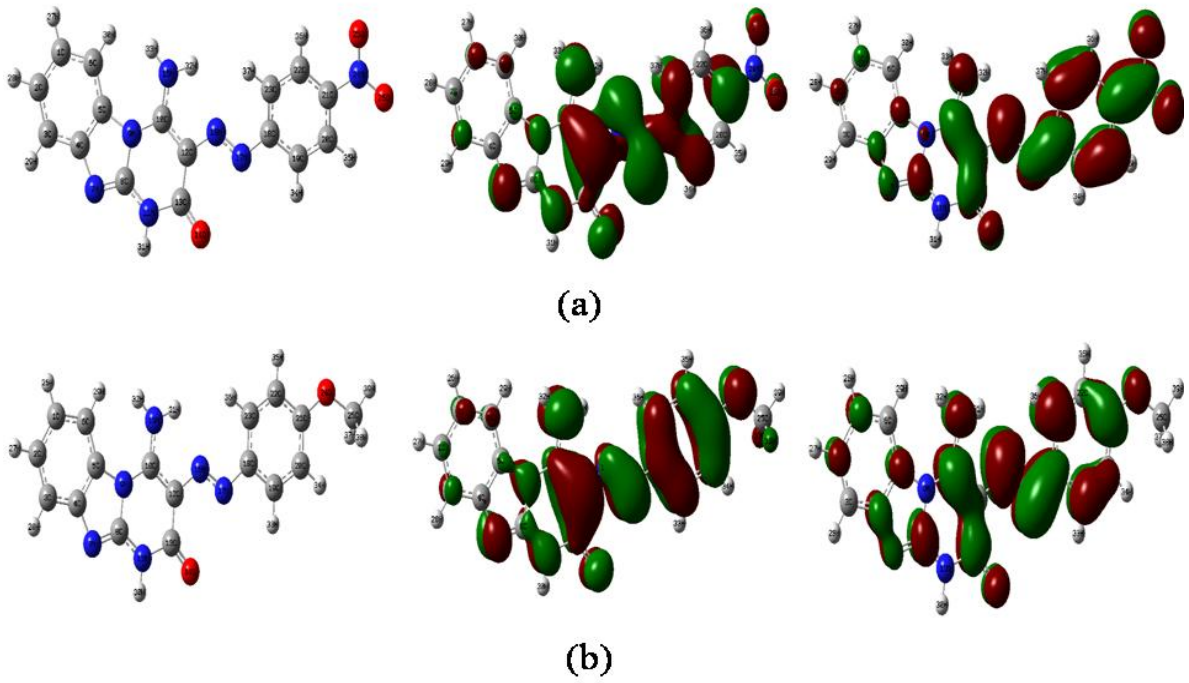

Figure 12. The optimized structure (left) and HOMO (center) and LUMO (right) distribution for molecules (a) NABIP (b) MABIP. [Atom legend: white = H; grey = C; blue = N; red = O]

Fe is considered as a soft acid and will co-ordinate to molecules having maximum softness and small energy gap ($\Delta E = E_{LUMO} - E_{HOMO}$). The quantum chemical parameters were calculated and summarized in Table 7. For the calculation of quantum chemical parameters the following equations were used [49].

$$\chi = -\frac{E_{LUMO} + E_{HOMO}}{2} \qquad (10)$$

$$\gamma = \frac{E_{\mathrm{LUMO}} - E_{\mathrm{HOMO}}}{2} \quad (11)$$

The inverse of the global hardness is designated as the softness, σ as follows:

$$\sigma = \frac{1}{\gamma} \quad (12)$$

where, hardness and softness measures the stability and reactivity of a molecule. Soft molecules are considered to be more reactive than hard ones because they can offer electron to acceptors easily. For the simplest transfer of electrons, adsorption could occur at the part of the molecule where σ which is a local property, has the highest value [49].

The fraction of electrons transferred (ΔN) was calculated by using equation [49]

$$\Delta N = \frac{\chi_{Fe} - \chi_{inh}}{2\left(\gamma_{Fe} + \gamma_{inh}\right)} \quad (13)$$

where a theoretical value of $\chi_{\mathrm{Fe}} \approx 4.06$ eV is taken for iron [49] and $\gamma_{\mathrm{Fe}} = 0$ is taken assuming that $I=A$ for bulk metals [50].

The Quantum chemical parameters for NABIP and MABIP are given in Table 7.

Table 7. Quantum chemical parameters for NABIP and MABIP.

Inhibitors	E_{HOMO} (eV)	E_{LUMO} (eV)	ΔE (eV)	μ (D)	γ (eV)	σ (eV^{-1})	ΔN	χ (eV)
MABIP	-5.6649	-1.2207	4.4442	5.425	1.7221	0.5807	0.1389	3.4428
NABIP	-6.3881	-1.1225	5.2656	4.3141	2.6328	0.3798	0.0579	3.7553

From Table 7 it is clear that MABIP has a higher value of E_{HOMO} (-5.6649 eV), σ (0.5807 eV^{-1}), ΔN (0.1389) and lower values of E_{LUMO} (-1.2207 eV), and energy gap (4.4442 eV) than NABIP. Thus, MABIP has more potency to get adsorbed on the mild steel surface resulting in a greater inhibition tendency than NABIP. Dipole moment values of MABIP and NABIP are 5.425 D and 4.3141 D respectively, which clearly suggest that these inhibitors are polar compounds and can easily donate electrons forming strong dπ-pπ bonding with the metal [51]. In the present study, the inhibition efficiency increases with the increasing dipole moment of the inhibitors, which could be attributed as higher polarity compounds will facilitate electrostatic interaction between the electric field due to the charged metal surface and electric moments of the inhibitors and contributes to their better adsorption

by influencing the transport process through the adsorbed layer [52]. Generally, Δ*N* indicates inhibition efficiency resulting from electron transfer from the inhibitor molecule to the iron atom. According to Lukovits's study [53], if the value of ΔN is < 3.6, the efficiency of inhibition increases with increasing electron donating ability of the inhibitor at the metal surface. An improvement in the electronic releasing power of MABIP was shown due to the presence of an electron donating substituent (–OCH_3 group) which improves the inhibition efficiency of MABIP. Figure 12(a, b), reveals that the HOMO location in both inhibitors is mostly distributed in the vicinity of the nitrogen of the imidazole ring, pyrimidine ring, NH_2 group, N=N group and oxygen of –OCH_3 and NO_2 group as well as phenyl ring attached to N=N group. LUMO location in both inhibitors is mostly distributed in the vicinity of the nitrogen of the N=N group, NH_2 group, NO_2 group and oxygen of –OCH_3 and NO_2 group as well as phenyl ring attached to N=N group. This indicates the reactive sites of the interaction between the inhibitor molecules and mild steel surface.

3.8. Mechanism of inhibition

Corrosion inhibition of mild steel in hydrochloric acid solution by both inhibitors (MABIP and NABIP) can be explained on the basis of molecular adsorption. These compounds inhibit corrosion by controlling both anodic as well as cathodic reactions. In acidic solutions these inhibitors exist as protonated species. In both inhibitors the nitrogen atoms present in the molecules can be easily protonated in an acidic solution and these protonated species are adsorbed on the cathodic sites of the mild steel and decrease the evolution of hydrogen. The adsorption on the anodic site occurs through π-electrons of pyrimidine, imidazole and phenyl rings and lone pair of electrons of nitrogen, and oxygen atoms present in both the inhibitors which decreases the anodic dissolution of mild steel.

4. CONCLUSIONS

(1) The synthesized phenylazopyrimidone dyes show good inhibition efficiencies for the corrosion of mild steel in a 15% HCl solution and the inhibition efficiency increases with an increase in the concentration of inhibitor. The inhibiting performance of MABIP is better than NABIP.

(2) The variation in the values of β_a and β_c (Tafel slopes) and the minor deviation of E_{corr} of inhibitors with respect to E_{corr} of the blank, indicates that both inhibitors tested are of mixed type in nature.

(3) EIS measurements show that the charge transfer resistance (R_{ct}) increases and double layer capacitance (C_{dl}) decreases in the presence of inhibitors, suggested the adsorption of the inhibitor molecules on the surface of mild steel.

(4) It is suggested from the results obtained from SEM, EDS, AFM, and the Langmuir adsorption isotherm that the mechanism of corrosion inhibition occurrs mainly through the adsorption process.

(5) Quantum chemical results of MABIP and NABIP show a higher value of E_{HOMO}, lower value of E_{LUMO}, and smaller value of ΔE, indicating that both inhibitors are good corrosion inhibitors for mild steel in hydrochloric acid.

ACKNOWLEDGEMENTS
The authors acknowledge University of KwaZulu-Natal for a postdoctoral scholarship for Dr I. Bahadur.

References

1. R. A. Prabhu, T. V. Venkatesha, A. V. Shanbhag, B. M. Praveen, G. M. Kulkarni, R. G. Kalkhambkar, *Mater. Chem. Phys.* 108 (2008) 283.
2. K. Mallaiya, R. Subramaniam, S. S. Srikandan, S. Gowri, N. Rajasekaran, A. Selvaraj, *Electrochim. Acta* 56 (2011) 3857.
3. D. D. N. Singh, T. B. Singh, B. Gaur, *Corros. Sci*. 37 (1995) 1005.
4. X. H. Li, S. D. Deng, H. Fu, T. H. Li, *Electrochim. Acta* 54 (2009) 4089.
5. A. Doner, E. A. Sahin, G. Kardas, O. Serindag, *Corros. Sci.* 66 (2013) 278.
6. M. A. Hegazy, A. M. Hasan, M. M. Emara, M. F. Bakr, A. H. Youssef, *Corros. Sci.* 65 (2012) 67.
7. M. Mahdavian, S. Ashhari, *Electrochim. Acta* 55 (2010) 1720.
8. M. Yadav, D. Behera, U. Sharma, *Corros. Eng. Sci. Technol*. 48 (2013) 19.
9. M. Yadav, D. Behera, S. Kumar, R. R. Sinha, *Ind. Eng. Chem. Res.* 5 (2013). 6318.
10. M. Yadav, U. Sharma, *J. Mater. Environ. Sci*. 2 (2011) 407.
11. M. Yadav, P. N. Yadav, U. Sharma, *Indian J. Chem. Technol.* 20 (2013) 363.
12. R. Solmaz, M. E. Mert, G. Kardas, B. Yazici, M. Erbil, *Acta Phys. Chem. Sinica* 24 (2008) 1185.
13. L. Tang, G. Mu, G. Liu. *Corros. Sci.* 45 (2003) 2251.
14. L. Tang, X. Li, G. Mu, G. Liu. *Appl. Surf. Sci*. 252 (2006) 6394.
15. E. E. Oguzie, *Mater. Chem. Phys*. 87 (2004) 212.
16. E. E. Oguzie, *Mater. Letts*. 59 (2005) 1076.
17. E. E. Ebenso, M. M. Kabanda, L. C. Murulana, A. K. Singh, S. K. Shukla *Ind. Eng. Chem. Res.* 51 (2012) 12940.
18. M. N. El-Haddad, A. S. Fouda, H. A. Mostafa, *J. Mater. Eng. Perform.* 22 (2013) 2277.
19. J. D. Talati, J. G. A. Patel, *Br. Corros. J*. 9 (1974) 181.
20. J. D. Talati, J. M. Pandya, *Anti-Corros. Methods. Mater*. 21 (1974) 7.
21. J. D. Talati, N. H. Joshi, *Werskt. Korros*. 31 (1980) 926.
22. S. S. Al-Juaid, *Port. Electrochim. Acta* 25 (2007) 363.
23. F. Karc, A. Demircal, I. Sener, T. Tilki, *Dyes and Pigments* 71 (2006) 90.
24. M. Lebrini, F. Robert, A. Lecante, C. Roos, *Corros. Sci.* 53 (2011) 687.
25. C. Lee, W. Yang, R. G. Parr, *Phys. Rev*. 37 (1988) 785.
26. D. Becke, *J. Chem. Phys.* 98 (1993) 1372.
27. D. Shuduan, X. Li, H. Fu, *Corros. Sci.* 53 (2011) 3596.
28. X. Wang, H. Yang, F. Wang, *Corros. Sci.* 53 (2011) 113.
29. X. Wang, H. Yang, F. Wang, *Corros. Sci.* 53 **(**2011) 113.
30. D. Jayaperumal, *Mater. Chem. Phys.* 119 (2010) 478.
31. E. S. Ferreira, C. Giancomlli, F. C. Giacomlli, A. Spinelli, *Mater. Chem. Phys*. 83 (2004) 129.
32. E. E. Ebenso, I. B. Obot, *Int. J. Electrochem. Sci*. 5 (2010) 2012.
33. L. Fragoza-Mar, O. Olivares-Xometl, M. A. Domínguez-Aguilar, E. A. Flores, P. Arellanes-Lozada, F. Jimenez-Cruz, *Corros. Sci*. 61 (2012) 171.

34. E. E. F. El-Sherbini, S. M. A. Wahaab, M. Deyab, *Mater. Chem. Phys.* 89 (2005) 183.
35. S. Ramesh, S. Rajeswari, *Electrochim. Acta* 49 (2004) 811.
36. H. Ashassi-Sorkhabi, B. Shaabani, D. Seifzadeh, *App. Surf. Sci*. 239 (2005) 154.
37. M. Behpour, S. M. Ghoreishi N. Mohammadi, N. Soltani, M. Salavati-Niasari *Corros Sci.* 52 (2010) 4046.
38. M. A. Amin, K. F. Khaled, Q. Mohsen, H. A. Arida, *Corros. Sci*. 52 (2010) 1684.
39. S. Ghareba, S. Omanovic, *Electrochim. Acta* 56 (2011) 3890.
40. I. Dehri, M. Ozcan, *Mater. Chem. Phys*. 98 (2006) 316.
41. E. E. Oguzie, *Corros. Sci.* 50 (2008) 2993.
42. S. V. Ramesh, V. Adhikari, *Bull. Mater. Sci*. 31 (2007) 699.
43. M. Behpour, S. M. Ghoreishi, N. Soltani, M. Salavati-Niasari, M. Hamadanian, A. Gandomi, *Corros. Sci*. 50 (2008) 2172.
44. X. Wang, H. Yang, F. Wang, *Corros. Sci.* 53 (2011) 113.
45. S. K. Shukla, M. A. Quraishi, *Corros. Sci.* 51 (2009) 1990.
46. M. Ozcan, *J. Solid State Electrochem*. 12 (2008) 1653.
47. S. Xia, M. Qiu, L. Yu, F. Liu, H. Zhao, *Corros. Sci*. 50 (2008) 2021.
48. V. S. Sastri, J. R. Perumareddi, *Corrosion* 53 (1997) 617.
49. R. G. Pearson, *Inorg. Chem*., 27 (1988) 734.
50. M. J. S. Dewar, W. Thiel, *J. Am. Chem. Soc*. 99 (1977) 4899.
51. I.B. Obot, N. O. Obi-Egbedi, *Mater. Chem. Phys.* 122 (2010) 325.
52. K. Babić-Samardžija, K. F. Khaled, N. Hackerman, *Appl. Surf. Sci.* 240 (2005) 327.
53. I. Lukovits, E. Klaman, F. Zucchi, *Corrosion* 57 (2001) 3.